Applied Catalysis B: Environmental 218 (2017) 538–544

Contents lists available at ScienceDirect

Applied Catalysis B: Environmental

journal homepage: www.elsevier.com/locate/apcatb

Carbon film encapsulated Pt NPs for selective oxidation of alcohols in acidic aqueous solution

Yanyan Sun [a], Xuewen Li [a], Jianguo Wang [b], Wensheng Ning [b], Jie Fu [a], Xiuyang Lu [a], Zhaoyin Hou [a,*]

[a] Key Laboratory of Biomass Chemical Engineering of Ministry of Education, Department of Chemistry, Zhejiang University, Hangzhou 310028, China
[b] State Key Laboratory Breeding Base of Green Chemistry-Synthesis Technology, Zhejiang University of Technology, Hangzhou 310032, China

ARTICLE INFO

Article history:
Received 19 March 2017
Received in revised form 25 May 2017
Accepted 29 June 2017
Available online 29 June 2017

Keywords:
Platinum catalyst
Encapsulation
Oxidation
Ethanol
Glycerol

ABSTRACT

Platinum is one of the best catalysts for various applications, but the deactivation of Pt nanoparticles (NPs) during alcohol oxidation is a major barrier to commercialization. In this work, multiwall carbon nanotubes supported carbon film encapsulated Pt NPs (Pt@C-MWCNTs) was synthesized and used in the selective oxidation of ethanol and glycerol in acidic aqueous solution. It was found that Pt@C-MWCNTs exhibited both higher activity and stability than bare Pt NPs. Characterization indicated that carbon film encapsulation can overcome the sintering, leaching and over-oxidation of Pt NPs during the reaction. Moreover, carbon film may also prevent the strong adsorption of organic carboxylic acid on Pt.

1. Introduction

Nanoparticles (NPs) possess high surface-to-volume ratio and unexpected properties as they are small enough to confine their electrons and produce quantum effects during the catalytic reaction [1,2]. At the same time, these catalysts can also be easily separated and recycled with more retention of catalytic activity. In recent years, "nanocatalysts" has become a term of the materials chemistry and catalysis community, which involves the use of materials at nanoscale dimensions as catalysts for a variety of heterogeneous catalysis applications [1]. The rapid development of nanotechnology has brought new challenges to conventional heterogeneous catalysts, and nanocatalysis has undergone an explosive growth during the past decade.Among of which, platinum NPs is one of the best catalysts for various applications, such as oxygen reduction reaction [3–6], biorefinery [7], VOCs oxidation [8,9], hydrogenation [10–12], selective oxidation of alcohols [13–17], catalytic hydrogenation and reforming in petrochemicals [18], fuel cells [19–23] and so on. But the deactivation of nano-sized Pt catalysts was often reported in selective oxidation and electro-oxidation of alcohols. In our previous works, it was found that the specific activity of surface Pt for the selective oxidation of glycerol decreased quickly from 341.5 h^{-1} (turnover frequency, at 10% conversion level of glycerol) to 214.0 h^{-1} (at 50% conversion level of glycerol) [13,24].

It was reported that metal leaching and sintering would bring the reconstruction of Pt, resulting in irreversible deactivation of Pt catalyst [25–27]. Over oxidation of Pt NPs would give rise to inactive oxide surface layer [28,29]. Moreover, strong adsorption of reactants, intermediates, products or byproducts during catalytic reactions would also induce the deactivation of metal catalyst because of the blockage of active sites surface by these strongly adsorbed molecules [14,25,30]. The deactivation of Pt catalysts during alcohol oxidation and electro-oxidation is a major barrier to commercialization and maintaining the stability of heterogeneous catalysts is difficult. Among these possible reasons, we think that the fatal reason for the deactivation of Pt catalyst during the selective oxidation of ethanol/glycerol might vary with the structure of catalyst and reaction conditions. And this proposition was seldom reported.

Recently, it was reported that graphene or carbon film encapsulated iron [31,32], FeCo alloy [33,34], CoNi alloy [35], Co, Fe_3C [36,37], Ru NPs [38], PtFe alloy [39] and Pt NPs [40–42], Pt nanocrystals embedded in MOFs [43,44], Pt NPs encapsulated in zirconia nanocage [45], $PtCu_3$ nanocages [46], Pt [47], Rh [48] or Ru NPs [49] confined inside carbon nanotubes can maintain their high activity and stability even in harsh conditions, as the strong interaction between the graphene layer and metals can retard its migration and sintering. And several graphene shells encapsulating metal NPs

* Corresponding author.
E-mail address: zyhou@zju.edu.cn (Z. Hou).

http://dx.doi.org/10.1016/j.apcatb.2017.06.086
0926-3373/

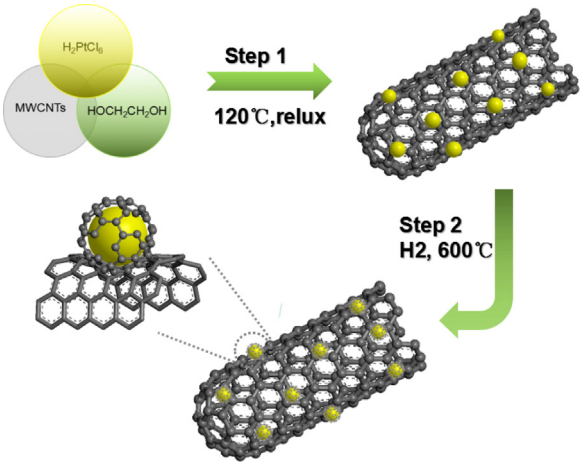

Scheme 1. Overall synthesis strategy of Pt@C-MWCNTs.

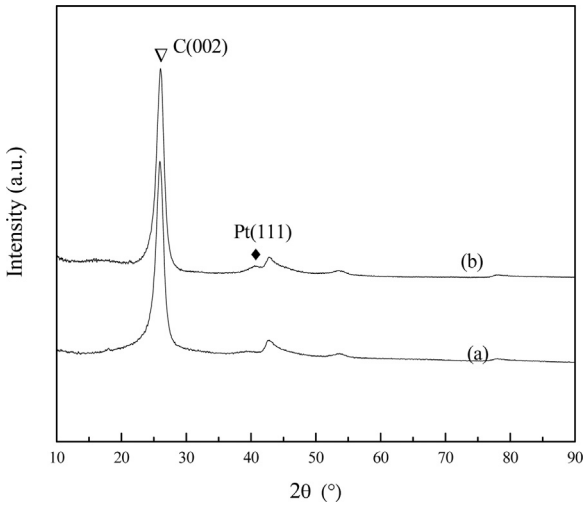

Fig. 1. XRD patterns of Pt/MWCNTs (a) and Pt@C-MWCNTs (b).

were reported in hydrogen evaluation reaction in acidic medium [50], triiodide reduction reaction in dye-sensitized solar cells, and catalytic oxidation and reduction reactions [51]. These findings paved a way for the concise preparation of stable nano-hybrid catalysts.

In this work, carbon film encapsulated Pt NPs supported on multi-wall carbon nanotubes (denoted as Pt@C-MWCNTs) was prepared in a facile routine in order to depress the deactivation of nano-sized Pt catalysts. The performance of Pt@C-MWCNTs for selective oxidation of ethanol and glycerol in acidic aqueous solution was carried out as model reactions, and compared with bare Pt/MWCNTs. It was found that Pt@C-MWCNTs exhibited both higher activity and stability than bare Pt NPs, and the fatal reason for the deactivation of bare Pt NPs was discussed.

2. Experiments

2.1. Catalyst preparation

MWCNTs (purity > 97%, diameter 30 ± 10 nm, and length less than 2 μm) used in this work were purchased from Shenzhen Nanotech Port Co. Ltd. (China). Before use, 6 g of raw MWCNTs were pretreated in 50 mL concentrated HNO_3 under refluxing at 70 °C for 12 h, washed with deionized water and dried in vacuum. And the acid −pretreated sample was denoted as H-MWCNTs.

The synthesis strategy of Pt@C-MWCNTs was illustrated in Scheme 1. At first, 0.2 g of H-MWCNTs and 0.27 mL aqueous solution of H_2PtCl_6 (0.01 g Pt/mL) were successively dispersed in a mixed solution of 20 mL ethylene glycol (EG, 99.5%, Sinopharm Chemical Reagent) and 5 mL deionized water under vigorous stirring for 1 h. And then, NaOH/EG solution (1 M) was added to above suspension to adjust its pH value to 11–12. Subsequently, the mixture was subjected to 120 °C and refluxed for 24 h to reduce platinum salt to metallic Pt. After reduction, the solid catalyst was isolated and washed with deionized water to remove residual chlorides. It was then extracted with ethanol for 5 h in a Soxhlet extractor. The solid was dried in vacuum at 60 °C and denoted as Pt/MWCNTs. At last, the dried Pt/MWCNTs was further treated in H_2 atmosphere at 600 °C for 1 h, and the final sample was denoted as Pt@C-MWCNTs.

Pt-based catalysts on other supports, such as SiO_2, MgO, Al_2O_3, ZnO and ZrO_2 were prepared similarly to above procedures. Before catalytic reaction, all catalysts were reduced in hydrogen at 200 °C for 1 h.

Actual content of Pt in prepared catalysts was determined on inductively coupled plasma-atomic emission spectroscopy (ICP-AES, Plasma-Spec- II spectrometer). The real content of Pt in the prepared Pt@C-MWCNTs and those of reference catalysts was summarized in Table S1.

2.2. Characterization

X-ray diffraction (XRD) analysis was performed on RIGAKUD/MAX2550/PC diffractometer using Cu Kα radiation at 40 kV and 100 mA. Diffraction data from 10 to 90° were obtained using continuous scanning at a speed of 0.02°/s and step 0.02°. Transmission electron microscopy (TEM, JEOL-2010F) was employed to observe the morphologies and dimensions of catalysts by using an accelerating voltage of 200 kV. Raman spectra was obtained using Renishaw 2000 Confocal Raman Microprobe (Renishaw Instruments, England) using 514.5 nm argon ion laser. X-ray photoelectron spectra (XPS) were recorded on Perkin-Elmer PHI ESCA System. X-ray source was Mg standard anode 146 (1253.6 eV) at 12 kV and 300 W.

Adsorption test of acetic acid on Pt/MWCNTs and Pt@C-MWCNTs was carried out in the following procedures: 0.1 g of fresh catalyst was dispersed in 20 mL acetic acid solution (0.06 g/mL) and stirred for 2 h to reach adsorption-desorption equilibrium, followed by centrifugation to separate the solid catalyst and supernatant liquid. Before Raman analysis, the solid catalyst was washed with deionized water for 5 times.

Temperature-programmed desorption of O_2 (O_2-TPD) over Pt/MWCNTs and Pt@C-MWCNTs was performed in a home-made microreactor equipped with a mass spectrometer (OmniStar GSD301, Switzerland). Samples (0.12 g) were first pretreated at 500 °C for 1 h and then cooled to room temperature in Ar, holding for 0.5 h. After that, the samples were cooled to 30 °C and exposed to 1% (v/v) O_2 (balanced with N_2). Then, the samples were purged by Ar at 30 °C for 60 min to an eliminate the physically adsorbed O_2 and then heated in Ar from 30 to 550 °C with a ramping rate of 10 °C min^{-1}. The concentration of O_2 (m/e = 32) in effluent was recorded by mass spectrometer

2.3. Catalytic oxidation of ethanol and glycerol

The performance of these catalysts for selective oxidation of ethanol was performed in a 100 mL custom designed stainless autoclave with a Teflon inner layer. A certain amount of catalyst and aqueous ethanol were added into the reactor. After closing the autoclave, it was charged with O_2. The reactor was then heated to a certain temperature, followed by starting the reaction via vigorous magnetic stirring. After the reaction, the autoclave was cooled

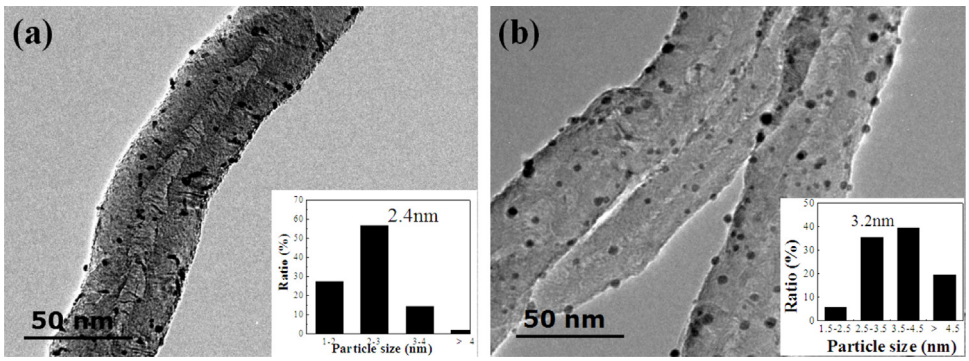

Fig. 2. TEM images of Pt/MWCNTs (a) and Pt@C-MWCNTs (b).

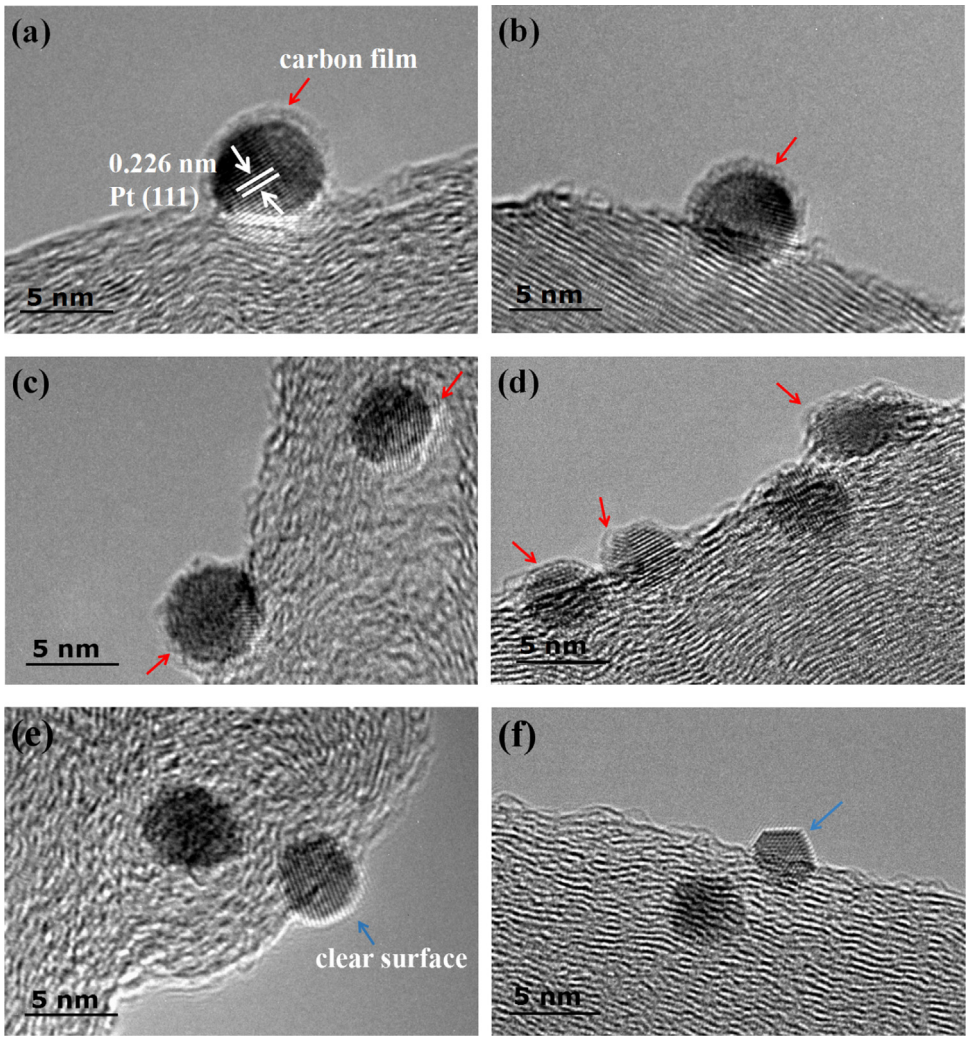

Fig. 3. HRTEM images of Pt@C-MWCNTs (a–d) and Pt/MWCNTs (e, f). (For interpretation of the references to colour in the text, the reader is referred to the web version of this article.)

to 0 °C. Gas in the effluent was collected and analyzed using the TCD gas chromatograph equipped with an APS-201 Flusin T column. Solid catalyst was separated by centrifugation and the liquid phase was analyzed by another gas chromatograph (HP 5890, USA) equipped with a 30 m capillary column (HP-5) and a flame ionization detector.

In the selective oxidation of glycerol, the aqueous solution was analyzed using an Agilent 1100 series high-performance liquid chromatograph (HPLC) equipped with a refractive index detector (RID) and a Zorbax SAX column (4.6 mm × 250 mm, Agilent). Product analysis method in detail could be found in our previous work [13].

Conversion was calculated as : (initial mmol of substrate − mmol of substrate left)/(initial mmol of substrate) × 100%.

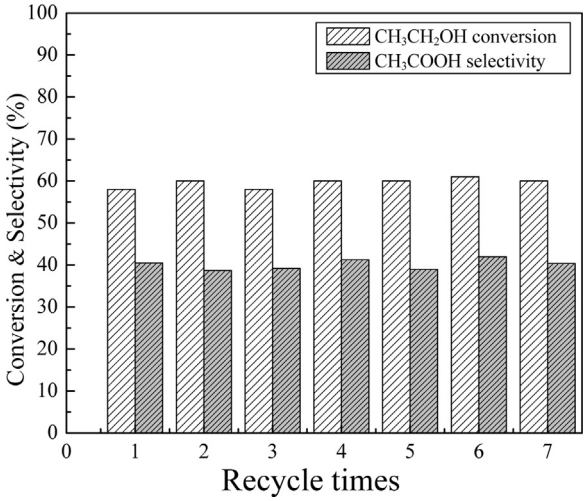

Fig. 4. Recycle usage of the Pt@C-MWCNTs for oxidation of ethanol. Reaction conditions: 20 mL aqueous solution of ethanol (0.20 g/mL), catalyst 30 mg, 2 MPa O_2, 130 °C, 2 h.

Selectivity was calculated as : (mmol of product in reaction mixture)/(initial mmol of substrate − mmol of substrate left) × 100%.

The turnover frequency (TOF) on the basis of total Pt atoms was calculated as : TOF = (number of substrate molecular converted)/(number of total Pt atoms)/(reaction time, h).

3. Results

3.1. The structure of catalysts

XRD analysis found that mainly a prominent peak was detected at 26°, indicating that MWCNTs remained its structure in both Pt/MWCNTs and Pt@C-MWCNTs. While the diffraction peak of Pt was weak and obscure, confirming that Pt NPs dispersed highly on the surface of MWCNTs (Fig. 1). And these uniformly dispersed NPs were further confirmed in their TEM images (Fig. 2). It was found that most Pt particles sized in 1.0–4.5 nm in Pt/MWCNTs, and the average size of 500 counted particles was 2.4 nm. On the other hand, the outline of Pt particles increased slightly to 1.5–6 nm in Pt@C-MWCNTs.

High-resolution TEM (HRTEM) analysis disclosed that most Pt NPs in Pt@C-MWCNTs were covered by a layer of carbon film (see Fig. 3a–d, red arrows), while mainly bare Pt particles with a clear surface were observed in Pt/MWCNTs (see Fig. 5e–f, blue arrows). It was postulated that the thin layer consisting of carbon species might be derived from the MWCNTs support during high-temperature pretreatment in a reducing atmosphere. The migration process of carbon species from support onto the surface of Pt particles could be explained via taking example by the nucleation and growth mechanism of carbon nanotubes or graphitic carbon nanofibers [52,53]. In such a high-temperature and reducing atmosphere, Pt NPs served as catalyst and nuclei upon which carbon film nucleated and grew. The growth mechanism involves catalytic decomposition of C—C bond in MWCNTs, followed by dissolution and diffusion of carbon atoms through the bulk of Pt particles. The final step involves the precipitation of carbon on the external surface of Pt particles. The growth of carbon film on Pt NPs induced conspicuous changes in the nanoparticles morphology, resulting in particles becoming rounder as carbon encapsulation progressed [54], as shown in Fig. 2 and Fig. S1(a, c).

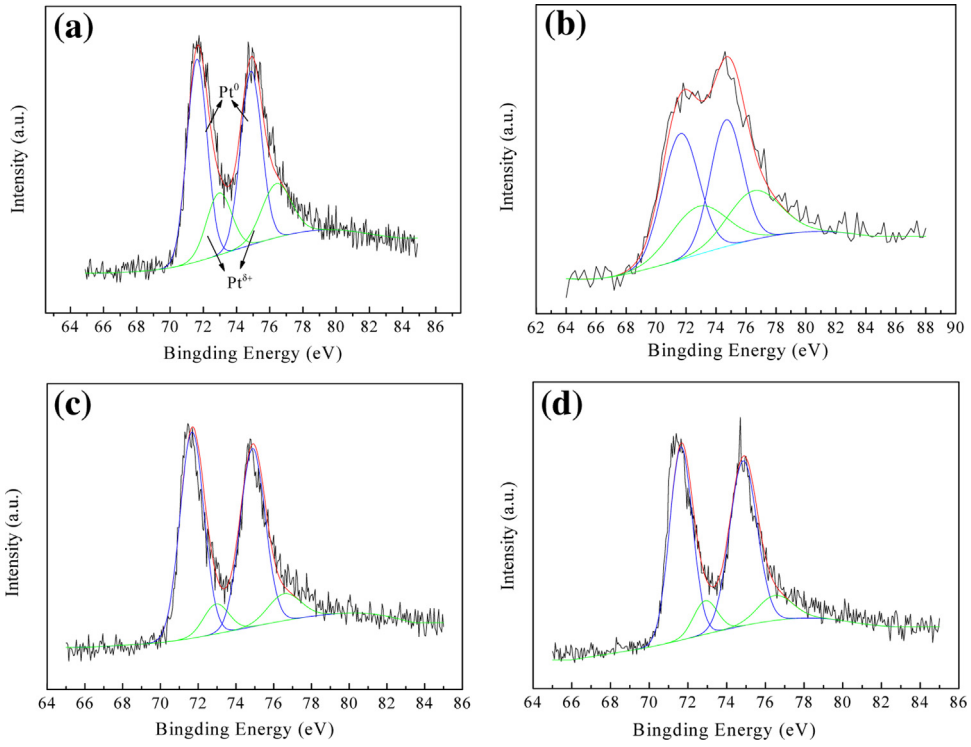

Fig. 5. XPS of Pt 4f of fresh (a), spent (b) Pt/MWCNTs, and fresh (c), spent (d) Pt@C-MWCNTs. (For interpretation of the references to colour in the text, the reader is referred to the web version of this article.)

Table 1
Oxidation of ethanol over different catalysts.[a]

Entry	Catalyst	Conv. (%)	Selectivity (%)		
			Acetaldehyde	Acetic acid	Ethyl acetate
1	Pt/MWCNTs	59.0	53.7	45.6	0.7
2	Pt@C-MWCNTs	72.1	32.9	66.4	0.7
3	Pt/SiO_2	50.6	56.3	42.9	0.8
4	Pt/MgO	4.5	100	0	0
5	Pt/Al_2O_3	7.3	100	0	0
6	Pt/ZnO	11.0	95.0	0	5.0
7	Pt/ZrO_2	19.3	95.1	0	4.5

[a] Reaction conditions: 12 mL aqueous solution of ethanol (0.15 g/mL), catalyst 10 mg, 2 MPa O_2, 130 °C, 2 h.

Table 2
Oxidation of glycerol over different catalysts.[a]

Catalyst	TOF (h^{-1})[b]	Conv. (%)	Selectivity (%)[c]			
			GLYA	DHA	GLYCA	Others
Pt/MWCNTs	63.6	30.2	82.3	16.3	0.8	0.6
Pt@C-MWCNTs	372.3	57.7	84.8	12.2	2.9	0.1

[a] Reaction conditions: 5 mL aqueous solution of glycerol (0.03 g/mL), catalyst 50 mg, 0.5 MPa O_2, 60 °C, 3 h.
[b] TOF was calculated on the basis of total Pt atoms when the conversion of glycerol was 20%.
[c] GLYA: glyceric acid, DHA: 1,3-dihydroxyacetone, GLYCA: glycolic acid, Others: CO_2 and CO was detected in gas effluent and oxalic acid in liquid phase.

3.2. Selective oxidation of ethanol and glycerol

Table 1 summarized the performance of Pt@C-MWCNTs, Pt/MWCNTs and traditional oxides (SiO_2, MgO, Al_2O_3, ZnO and ZrO_2) supported Pt catalysts for the selective oxidation of ethanol in an acidic aqueous solution. It was found that Pt@C-MWCNTs exhibited predominant performance for the oxidation of ethanol among all tested catalysts, the selectivity of acetic acid reached 66.4% with a 72.1% conversion of ethanol, and the calculated turnover frequency (TOF) of total Pt atoms reached 26706 h^{-1} (at 130 °C, 2 h).

On the other hand, the conversion of ethanol and selectivity of acetic acid over Pt/MWCNTs decreased to 59.0 and 45.6%, respectively. And the calculated TOF of total Pt also decreased to 21644 h^{-1}. These results indicated that carbon film encapsulated Pt NPs were more active for the oxidation of ethanol with molecular oxygen in acidic aqueous solution. Most importantly, Pt@C-MWCNTs was extremely stable, and the detected conversion of ethanol and the selectivity of acetic acid changed minor in the consecutive seven recycle experiments (see Fig. 4). As references, traditional oxides supported Pt catalysts can catalyze the oxidation of ethanol, but mainly acetaldehyde formed over MgO, Al_2O_3, ZnO and ZrO_2 supports. These results demonstrated that the nature of support played a crucial role in the activity and selectivity of selective oxidation of ethanol. And the excellent performance of Pt@C-MWCNTs was further confirmed under varied reaction temperature (see Fig. S2) and reaction time (see Fig. S3).

The excellent performance of Pt@C-MWCNTs was also confirmed in the selective oxidation of glycerol in an acidic aqueous solution (see Table 2). The detected conversion of glycerol over Pt@C-MWCNTs was higher than that of Pt/MWCNTs, and the calculated TOF (at 20% conversion level) on the basis of total Pt atoms was 63.6 and 372.3 h^{-1}, respectively.

Time course curve of the selective oxidation of glycerol indicated that the conversion of glycerol increased continuously with reaction time over Pt@C-MWCNTs (see Fig. S4(a)), but the detected conversion of glycerol over Pt/MWCNTs increased slowly under the same conditions. The calculated reaction rate (R) at different concentration of glycerol (C_{GLY}) further confirmed that the reaction rate on Pt/MWCNTs decreased to near zero when C_{GLY} decreased to 17.9 mg/mL (nearly 60% of the initial C_{GLY}). On the other hand, the reaction rate over Pt@C-MWCNTs was 5.5 mg/mL/h under the same C_{GLY} (see Fig. S4(b)). The deactivation of Pt/MWCNTs with time could be attributed to that Pt particles were occupied by the strongly-adsorbed organic carboxylic acid generated during the reaction (see Fig. S4(c)) and/or over oxidation of Pt atoms by O_2.

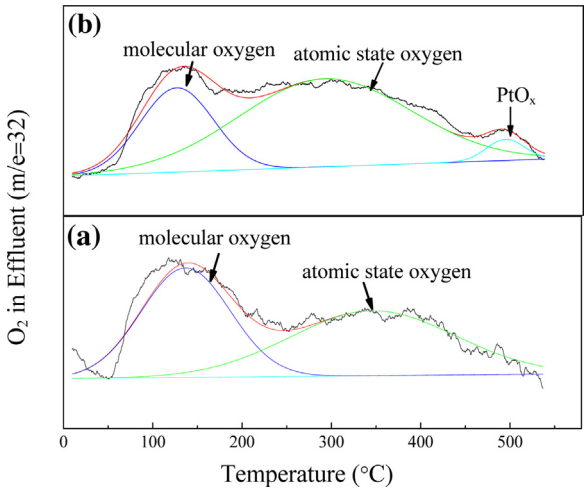

Fig. 6. O_2–TPD profiles of (a) Pt@C-MWCNTs and (b) Pt/MWCNTs catalysts.

4. Discussions

According to the pioneering works of Davis et al. [25], Pt catalysts suffered of deactivation during the reaction either because of leaching, sintering, over oxidation of Pt NPs to inactive oxide surface layer or strong adsorption of products or reactant. A series of controlled experiments were carried out in order to explain the higher activity and stability of Pt@C-MWCNTs.

At first, the content of Pt in spent Pt/MWCNTs and Pt@C-MWCNTs was detected and summarized in Table S1 (see entry 2, 4). It was found that the detected amount of Pt in spent Pt/MWCNTs decreased slightly from 1.04 to 0.94 wt%, but the content of Pt in spent Pt@C-MWCNTs remained stable, indicating that carbon film encapsulated Pt NPs was more stable in the acidic aqueous solution. TEM images also confirmed that leaching and sintering would happen in spent Pt/MWCNTs (see Fig. S1(a, b)), but it was quite interesting to note that Pt NPs still dispersed evenly in the 7 times

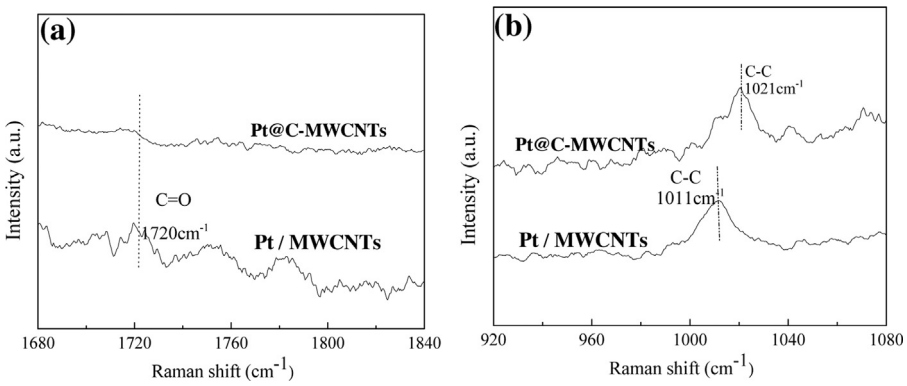

Fig. 7. Raman analysis of adsorbed acetic acid on Pt/MWCNTs and Pt@C-MWCNTs.

recycled Pt@C-MWCNTs. It might be attributed to the fact that carbon film retarded the leaching and sintering of Pt NPs.

Fig. 5 compared the binding energy of Pt 4f in fresh and spent Pt/MWCNTs (Fig. 5(a, b)) and Pt@C-MWCNTs (Fig. 5(c, d)). The spectra of Pt 4f can be deconvoluted into two pairs of doublets, and one doublet with the binding energy of 71.6 (Pt $4f_{7/2}$) and 74.8 eV (Pt $4f_{5/2}$) could be assigned to metallic Pt^0, while the other doublet around 72.9 (Pt $4f_{7/2}$) and 76.4 eV (Pt $4f_{5/2}$) corresponded to $Pt^{\delta+}$ [24,55]. The relative proportion of Pt species was estimated from their relative deconvoluted peaks areas, which was summarized in Table S2. It is found that the proportion of $Pt^{\delta+}$ in spent Pt/MWCNTs increased obviously from 28.4 to 37.0%, which indicated that over-oxidation of Pt NPs would happen during the reaction process. While the proportion of $Pt^{\delta+}$ in spent Pt@C-MWCNTs only increased slightly from 14.0 to 15.8%. That is, carbon film encapsulated Pt NPs would suppress over-oxidation of Pt NPs during the reaction process.

Temperature-programmed desorption of O_2 (O_2-TPD) over Pt/MWCNTs and Pt@C-MWCNTs catalysts also indicated that mainly molecular oxygen (peak β_1) and atomic oxygen (peak β_2) adsorbed on the surface of carbon film encapsulated Pt NPs (Pt@C-MWCNTs, see Fig. 6). But on the surface of bare Pt NPs, oxygen from over oxidized PtO_2 species was detected at 510–530 °C (peak β_3) [56,57]. This strongly adsorbed oxygen on bare Pt NPs would occupy the surface with the most active sites, giving rise to the fact that substrate molecules (ethanol or glycerol) cannot access to active surface and bring deactivation.

Adsorption tests of acetic acid on Pt/MWCNTs and Pt@C-MWCNTs were performed to investigate adsorption properties of carboxylic acid (main product in oxidation of ethanol and glycerol) on catalysts. Raman analysis of catalysts adsorbed with acetic acid indicated that a large amount of acetic acid were adsorbed on the bare surface of Pt catalyst (Pt/MWCNTs); while no obvious adsorption of acetic acid was observed on Pt@C-MWCNTs (see Fig. 7(a), $\nu_{(C=O)}$ vibrations). The calculated saturated adsorption capacity of acetic acid over Pt/MWCNTs and Pt@C-MWCNTs was 2.4 and 1.0 g-acetic acid/g-catalyst, respectively. It might be attributed to the strong coordination adsorption of acetic acid in the form of acetate species on the bare surface of Pt NPs [58,59], but carbon film encapsulated out of Pt NPs would hinder the coordination of acetic acid, bringing about relatively lower adsorption capacity. The Raman shift at 1021 cm^{-1} (see Fig. 7(b)) was assigned to $\nu_{(C-C)}$ vibrations of the absorbed acetate species [60]. The lower Raman shift for Pt/MWCNTs (1011 cm^{-1}) than that of Pt@C-MWCNTs (1021 cm^{-1}) gave a further explanation that the strong coordination adsorption of acetic acid on bare Pt NPs would weaken the C—C bond strength to some extent.

Above analysis confirmed that the strong adsorption of acetic acid generated during ethanol oxidation on the bare surface of Pt NPs did occur, which gave rise to competitive adsorption on active sites between organic acid and substrate and inhibition of alcohol oxidation process. Matthew et al. [30] also observed that the addition of organic acid (acetic acid and propionic acid) would inhibited the initial oxidation rate of 1,6-hexanediol as result of the competitive adsorption of the organic acid on the platinum surface. The addition of acetic acid has also been shown to decrease the conversion rate of 5-Hydroxymethylfurfural [61] and glycerol [14] oxidation over Pt/C in acidic conditions. Moreover, Kapkowski e al [62]. found that silica encapsulated Au NPs can prevent the excess adsorption of the acidic products, and higher conversion (100%) and acetic acid yield (90%) were observed over silica encapsulated Au ($0.1Au/SiO_2$) in deep glycerol oxidation in diluted solutions than the high Au content counterpart without encapsulation.

5. Conclusions

Carbon film encapsulated Pt NPs supported on MWCNTs was found to possess higher activity and stability in the oxidation of ethanol and glycerol comparing to bare Pt catalyst. No sintering or leaching of Pt was observed on Pt@C-MWCNTs after seven recycles in the oxidation of ethanol, which were ascribed to that carbon film could retard the sintering of Pt NPs and prevented it from leaching. XPS analysis of the fresh and spent Pt/MWCNTs and Pt@C-MWCNTs confirmed that over oxidation did happen in bare Pt NPs, but carbon film encapsulating on the outside of Pt NPs would suppress the over oxidation of Pt NPs when exposed to O_2 atmosphere. O_2-TPD also indicated that strongly adsorbed oxygen would bring the formation of over-oxidized PtO_2 species on the surface of bare Pt NPs. Raman analysis of acetic acid-adsorbed Pt/MWCNTs and Pt@C-MWCNTs implied that a large amount of acetic acid generated in ethanol oxidation would adsorb on the surface of bare Pt NPs, giving rise to competitive adsorption on active sites between organic acid and substrate and inhibited alcohol oxidation process.

Acknowledgements

This work was financially supported by the National Natural Science Foundation of China (Contract Nos. 21473155, 21273198) and Natural Science Foundation of Zhejiang Province (Contract No. L12B03001).

Appendix A. Supplementary data

Supplementary data associated with this article can be found, in the online version, at http://dx.doi.org/10.1016/j.apcatb.2017.06.086.

References

[1] H. Zeng, Acc. Chem. Res. 46 (2013) 226–235.
[2] A.T. Bell, ChemInform 299 (2003) 1688–1691.
[3] K. Huang, K. Sasaki, R.R. Adzic, Y. Xing, J. Mater. Chem. 22 (2012) 16824–16832.
[4] M. Nesselberger, S. Ashton, J.C. Meier, I. Katsounaros, K.J.J. Mayrhofer, M. Arenz, J. Am. Chem. Soc. 133 (2011) 17428–17433.
[5] N.E. Sahin, T.W. Napporn, L. Dubau, F. Kadirgan, J.-M. Léger, K.B. Kokoh, Appl. Catal. B: Environ. 203 (2017) 72–84.
[6] R.A.M. Esfahani, S.K. Vankova, A.H.A.M. Videla, S. Specchia, Appl. Catal. B: Environ. 201 (2017) 419–429.
[7] Y. Wang, S. Agarwal, H.J. Heeres, ACS Sustainable Chem. Eng. 5 (2017) 469–480.
[8] H.-J. Sedjame, C. Fontaine, G. Lafaye, J. Barbier Jr., Appl. Catal. B: Environ. 144 (2014) 233–242.
[9] Z. Abdelouahab-Reddam, R.E. Mail, F. Coloma, A. Sepúlveda-Escribano, Appl. Catal. A: Gen. 494 (2015) 87–94.
[10] R. Nie, J. Wang, L. Wang, Y. Qin, P. Chen, Z. Hou, Carbon 50 (2012) 586–596.
[11] D.D. Falcone, J.H. Hack, A.Y. Klyushin, A. Knop-Gericke, R. Schlögl, R.J. Davis, ACS Catal. 5 (2015) 5679–5695.
[12] C.J. Kliewer, C. Aliaga, M. Bieri, W. Huang, C.-K. Tsung, J.B. Wood, K. Komvopoulos, G.A. Somorjai, J. Am. Chem. Soc. 132 (2010) 13088–13095.
[13] D. Liang, J. Gao, H. Sun, P. Chen, Z. Hou, X. Zheng, Appl. Catal. B: Environ. 106 (2011) 423–432.
[14] B.N. Zope, R.J. Davis, Green Chem. 13 (2011) 3484–3491.
[15] R. Rizo, D. Sebastián, M.J. Lázaro, E. Pastor, Appl. Catal. B: Environ. 200 (2017) 246–254.
[16] G. Long, X. Li, K. Wan, Z. Liang, J. Piao, P. Tsiakaras, Appl. Catal. B: Environ. 203 (2017) 541–548.
[17] J.W. Magee, W. Zhou, M.G. White, Appl. Catal. B: Environ. 152–153 (2014) 397–402.
[18] J. Gu, Z. Zhang, P. Hu, L. Ding, N. Xue, L. Peng, X. Guo, M. Lin, W. Ding, ACS Catal. 5 (2015) 6893–6901.
[19] H. Wang, R. Wang, H. Li, Q. Wang, J. Kang, Z. Lei, Int. J. Hydrogen Energy 36 (2011) 839–848.
[20] Z. Xu, H. Zhang, H. Zhong, Q. Lu, Y. Wang, D. Su, Appl. Catal. B: Environ. 111–112 (2012) 264–270.
[21] M. Laurent-Brocq, N. Job, D. Eskenazi, J.-J. Pireaux, Appl. Catal. B: Environ. 147 (2014) 453–463.
[22] X. Peng, S. Zhao, T.J. Omasta, J.M. Roller, W.E. Mustain, Appl. Catal. B: Environ. 203 (2017) 927–935.
[23] G. Cognard, G. Ozouf, C. Beauger, G. Berthomé, D. Riassetto, L. Dubau, R. Chattot, M. Chatenet, F. Maillard, Appl. Catal. B: Environ. 201 (2017) 381–390.
[24] R. Nie, D. Liang, L. Shen, J. Gao, P. Chen, Z. Hou, Appl. Catal. B: Environ. 127 (2012) 212–220.
[25] M.S. Ide, D.D. Falcone, R.J. Davis, J. Catal. 311 (2014) 295–305.
[26] J. Im, M. Choi, ACS Catal. 6 (2016) 2819–2826.
[27] M.H. Wiebenga, C.H. Kim, S.J. Schmieg, S.H. Oh, D.B. Brown, D.H. Kim, J.-H. Lee, C.H.F. Peden, Catal. Today 184 (2012) 197–204.
[28] H.A. Rass, N. Essayem, M. Besson, Green Chem. 15 (2013) 2240–2251.
[29] C. Mondelli, J.-D. Grunwaldt, D. Ferri, A. Baiker, Phys. Chem. Chem. Phys. 12 (2010) 5307–5316.
[30] M.S. Ide, R.J. Davis, J. Catal. 308 (2013) 50–59.
[31] J. Wang, G. Wang, S. Miao, J. Li, X. Bao, Faraday Discuss. 176 (2014) 135–151.
[32] D. Deng, L. Yu, X. Chen, G. Wang, L. Jin, X. Pan, J. Deng, G. Sun, X. Bao, Angew. Chem. Int. Ed. 52 (2013) 371–375.
[33] J. Deng, P. Ren, D. Deng, L. Yu, F. Yang, X. Bao, Energy Environ. Sci. 7 (2014) 1919–1923.
[34] J. Deng, L. Yu, D. Deng, X. Chen, F. Yang, X. Bao, J. Mater. Chem. A 1 (2013) 14868–14873.
[35] J. Deng, P. Ren, D. Deng, X. Bao, Angew. Chem. Int. Ed. 54 (2015) 2100–2104.
[36] J. Shi, Y. Wang, W. Du, Z. Hou, Carbon 99 (2016) 330–337.
[37] Y. Hu, J.O. Jensen, W. Zhang, L.N. Cleemann, W. Xing, N.J. Bjerrum, Q. Li, Angew. Chem. Int. Ed. 53 (2014) 3675–3679.
[38] J. Shi, M. Zhao, Y. Wang, J. Fu, X. Lu, Z. Hou, J. Mater. Chem. A 4 (2016) 5842–5848.
[39] D.Y. Chung, S.W. Jun, G. Yoon, S.G. Kwon, D.Y. Shin, P. Seo, J.M. Yoo, H. Shin, Y.-H. Chung, H. Kim, B.S. Mun, K.-S. Lee, N.-S. Lee, S.J. Yoo, D.-H. Lim, K. Kang, Y.-E. Sung, T. Hyeon, J. Am. Chem. Soc. 137 (2015) 15478–15485.
[40] L. Gao, Q. Fu, J. Li, Z. Qu, X. Bao, Carbon 101 (2016) 324–330.
[41] H. Kim, A.W. Robertson, S.O. Kim, J.M. Kim, J.H. Warner, ACS Nano 9 (2015) 5947–5957.
[42] L. Guo, W.J. Jiang, Y. Zhang, J.S. Hu, Z.D. Wei, L.J. Wan, ACS Catal. 5 (2015) 2903–2909.
[43] K. Na, K.M. Choi, O.M. Yaghi, G.A. Somorjai, Nano Lett. 14 (2014) 5979–5983.
[44] K.M. Choi, K. Na, G.A. Somorjai, O.M. Yaghi, J. Am. Chem. Soc. 137 (2015) 7810–7816.
[45] N. Cheng, M.N. Banis, J. Liu, A. Riese, X. Li, R. Li, S. Ye, S. Knights, X. Sun, Adv. Mater. 27 (2015) 277–281.
[46] B.Y. Xia, H.B. Wu, X. Wang, X.W. Lou, J. Am. Chem. Soc. 134 (2012) 13934–13937.
[47] F. Zhang, F. Jiao, X. Pan, K. Gao, J. Xiao, S. Zhang, X. Bao, ACS Catal. 5 (2015) 1381–1385.
[48] X. Pan, Z. Fan, W. Chen, Y. Ding, H. Luo, X. Bao, Nat. Mater. 6 (2007) 507–511.
[49] X. Pan, X. Bao, Acc. Chem. Res. 44 (2011) 553–562.
[50] X. Zou, X. Huang, A. Goswami, R. Silva, B.R. Sathe, E. Mikmeková, T. Asefa, Angew. Chem. Int. Ed. 126 (2014) 4372–4376.
[51] T. Fu, M. Wang, W. Cai, Y. Cui, F. Gao, L. Peng, W. Chen, W. Ding, ACS Catal. 4 (2014) 2536–2543.
[52] P. Nikolaev, M.J. Bronikowski, R.K. Bradley, F. Rohmund, Chem. Phys. Lett. 313 (1999) 91–97.
[53] K.P. De Jong, J.W. Geus, Cat. Rev. Sci. Eng. 42 (2000) 481–510.
[54] J. Wu, S. Helveg, S. Ullmann, Z. Peng, A.T. Bell, J. Catal. 338 (2016) 295–304.
[55] J.H. Kim, S.M. Choi, S.H. Nam, M.H. Seo, S.H. Choi, W.B. Kim, Appl. Catal. B: Environ. 82 (2008) 89–102.
[56] A. Katsaounis, Z. Nikopoulou, X.E. Verykios, C.G. Vayenas, J. Catal. 222 (2004) 192–206.
[57] X. Fu, Y. Liu, W. Yao, Z. Wu, Catal. Commun. 83 (2016) 22–26.
[58] M. Heinen, Z. Jusys, R.J. Behm, J. Phys. Chem. C 114 (2010) 9850–9864.
[59] D.S. Corrigan, E.K. Krauskopf, L.M. Rice, A. Wieckowski, M.J. Weaver, J. Phys. Chem. 92 (1988) 1596–1601.
[60] M.H. Brijaldo, H.A. Rojas, J.J. Martinez, F.B. Passos, J. Catal. 331 (2015) 63–75.
[61] M.A. Lilga, R.T. Hallen, M. Gray, Top. Catal. 53 (2010) 1264–1269.
[62] M. Kapkowski, P. Bartczak, M. Korzec, R. Sitko, J. Szade, K. Balin, J. Lelątko, J. Polanski, J. Catal. 319 (2014) 110–118.